AIAA JOURNAL
Vol. 37, No. 10, October 1999

Counter-Rotating Vortices Embedded in a Turbulent Boundary Layer with Inclined Jets

X. Zhang*
University of Southampton, Southampton, England SO17 1BJ, United Kingdom

Counter-rotating vortex pairs in an otherwise flat-plate turbulent boundary layer were studied in a wind-tunnel model experiment. The vortices were produced with pairs of inclined round jets with nozzle exit flush with the plate surface. The skew angle and pitch angle of the nozzle were 45 deg. The Reynolds number based on the momentum thickness of the oncoming boundary layer was 3.8×10^3. A velocity field survey was performed with a three-component laser Doppler anemometry system. The effects of jet speed on the streamwise development of the vortices were investigated. The flow had an upwash region in between the vortices that were embedded in the turbulent boundary layer. The upwash was produced by the vortices and the interaction between diametrically opposed secondary, near-wall flows. Velocity measurements indicated flow separation and entrainment behind the jet exit, and this was corroborated by surface flow observation. The vortex development was divided into two stages: a near-field stage where the wake of the jet plays an important role and a far-field stage where turbulent dissipation and diffusion are important.

Nomenclature

D	= nozzle hydraulic diameter
U, V, W	= mean velocity components in x, y, z directions
x, y, z	= Cartesian coordinates
α	= jet pitch angle
β	= jet skew angle
Γ	= circulation level, normalized by U_∞/D^3
λ	= jet velocity ratio, V_j/U_∞
Ω	= normalized streamwise vorticity, $(\partial W/\partial y - \partial V/\partial z)D/U_\infty$

Subscripts

c	= center of the vortex
j	= jet flow condition
m	= peak vorticity
∞	= freestream condition

I. Introduction

WALLIS[1] suggested that a judicious use of inclined jets can produce discrete streamwise vortices and hence create possibilities for flow control, particularly in situations where a boundary layer separates or stall occurs. Various concepts such as corotating jets and jet vanes were proposed by Wallis, which were later taken up independently by Freestone[2] and Johnston and Nishi,[3] using wind-tunnel model tests. Since then, a number of experimental studies have been performed on the inclined jets (or jet vortex generators).[4–7] The main advantage of using inclined jets over conventional vanes (see, for example, Ref. 8) is a lower and possibly zero drag penalty when not activated, and a potential for active control.

The generation and development of a streamwise vortex or vortices by inclined jets are determined by a number of flow parameters, such as skew angle, pitch angle, velocity ratio, relative size and geometry of the jet, and nozzle orientation. Among the various researchers Freestone[2] surmised that a rectangular nozzle could produce a superior vortex for flow control, following suggestions made by Wallis.[1] Johnston and Nishi[3] and Compton and Johnston[4] conducted detailed surface-pressure and pressure-probe surveys of single- and multiple-jet vortex generators, including the effects of the skew angle and velocity ratio. Selby et al.[5] identified the effects of jet speed and skew angle on flow separation over a ramp, using surface-pressure tappings and oil-flow visualization. Zhang and Collins[6,7] studied the effects of skew angle, pitch angle, and jet speed using a single round jet and a single rectangular jet in a flat-plate boundary layer, employing laser Doppler anemometry (LDA).

Introducing a skew angle leads to a single, dominant streamwise vortex eventually being formed downstream of a nozzle. The strength of the vortex is influenced greatly by the skew angle. Selby et al.[5] identified an optimal skew angle between 60 deg $\leq \beta \leq$ 90 deg, whereas Compton and Johnston[4] suggested a value between 45 deg $\leq \beta \leq$ 90 deg. Zhang and Collins[6,7] gave a value between 30 deg $\leq \beta \leq$ 60 deg for effective flow control. Apart from the skew angle, a pitch angle of 30 deg was found to produce stronger streamwise vortices. It was also shown that a higher jet speed would not necessarily result in better vortices for flow control, as the center of the vortex is farther away from the aerodynamic surface than those produced with slower jets.

In recent works a significant amount of effort has been concentrated on a single jet or jet arrays producing corotating vortices. One feature of the corotating vortices is the ability of the vortices to stay closer to an aerodynamic surface. The current study, however, focuses on inclined jet pairs producing counter-rotating vortices in a boundary layer, which is an area that has received little attention up until now. Johnston and Nishi[3] found jet arrays that gave counter-rotating vortices, which could cause significant spanwise skin-friction variation. If properly arranged, the jets can lead to stronger vortices initially, which would further enhance the prospect of employing bleed air from an aircraft engine or exhaust of a racing car for flow control. In fact, a counter-rotating arrangement is ideally suited to diffuser flow control applications such as that on a racing car. A relevant study on a counter-rotating vortex pair above an aerodynamic surface was performed by Cutler and Bradshaw[9] using a delta wing to generate the vortices. The difference between the current study and that of Cutler and Bradshaw is that the vortices employed in this study are at least an order magnitude lower in terms of circulation level. The current work investigates the use of vortices for flow control; those employed by Cutler and Bradshaw are typical of vortex/aircraft interaction. Furthermore, the streamwise vortices generated by an inclined jet will not possess a velocity deficiency in the core of the vortex if the jet velocity ratio λ is higher than unity.[4] Another feature of the present flow is the direction of the transverse velocity in between the vortices. Counter-rotating vortices generated by delta wings and similar devices tend to have a

Received 9 September 1998; revision received 23 February 1999; accepted for publication 11 March 1999.

*Senior Lecturer, Department of Aeronautics and Astronautics. Senior Member AIAA.

common flow down in between the vortices. In the present study there exists a common flow up in between the vortices. As a result, the effective area for flow control differs. Another related study using vanes was performed by Pauley and Eaton,[10] where a common flow down region also existed between the vortices.

The approach used in this study is that of wind-tunnel model experiments. To establish an understanding of major flow physics, a baseline flow including a flat-plate turbulent boundary layer and inclined jets was selected. A detailed description of the experimental arrangement is given in Sec. II.A.

II. Experimental Setup

A. Test Conditions

The model tests were conducted in the R. J. Mitchell (3.5 × 2.6 m) low-speed wind tunnel in the Department of Aeronautics and Astronautics. This tunnel has a freestream turbulence level of 0.3%, and the tests were run at a tunnel speed of 20 m/s. The flat-plate boundary layer was developed on an aluminium plate placed at 0.9 m above the tunnel floor with a leading-edge droop formed by a 55-mm circular arc with a 125-mm radius. The plate occupied the span of the test section, and the two-dimensionality of the flow was verified at various spanwise positions. Transition was fixed by a 10-mm-wide 60-grit sand strip placed 100 mm downstream of the leading edge. A schematic of the test setup is shown in Fig. 1. The jets were placed 1.07 m downstream of the sand strip. The boundary layer 100 mm upstream of the jet center (origin of the measurement coordinates) has a momentum thickness of 2.74 mm and a skin-friction coefficient of 0.003, corresponding to a fully developed turbulent boundary layer. The thickness of the boundary layer is 25 mm. The Reynolds number based on the momentum thickness is 3.8×10^3. The Reynolds number based on the jet diameter is in the range of 9.7×10^3–2.9×10^4.

The arrangement of the inclined nozzles is shown in Fig. 1a, together with the measurement coordinate system that is used in the presentation of the results. A total of three pairs of inclined nozzles was employed. Measurements were concentrated on the central pair. This arrangement serves to establish proper boundary conditions for numerical modeling exercises. The nozzles were formed by 100-mm straight brass pipes 14 mm in diameter. The pipes were installed into a plug that was flush mounted on the plate. The nozzles were connected through a plastic pipe to a Dantec 55L18 seeding generator and through the generator to a Fisher valve that led to a compressed air supply. The pressure was thus regulated twice in a test and stayed stable throughout a run (lasting typically 1 h). The jet velocity was calibrated before and after each test run using a pitot-static probe. The pitch angle α and the skew angle β of the jet were both set at 45 deg, following results from earlier, single-jet studies.[6,7] The velocity ratios of the jet λ were set at 0.5, 1.0, and 1.5. For each flow setting measurements were conducted on cross planes at $x = 5$, 10, 20, 30, and $40D$, as well as on a rectangular area at $z = 0.25D$ above the nozzle exit. Furthermore, a series of spanwise velocity surveys were performed at a height of $z = 0.25D$ at various streamwise locations (5–$40D$). When surface flow visualizations were performed, the model surface was covered by a black Fablon self-adhesive vinyl sheet, on top of which a mixture of fluorescence powder and paraffin was applied.

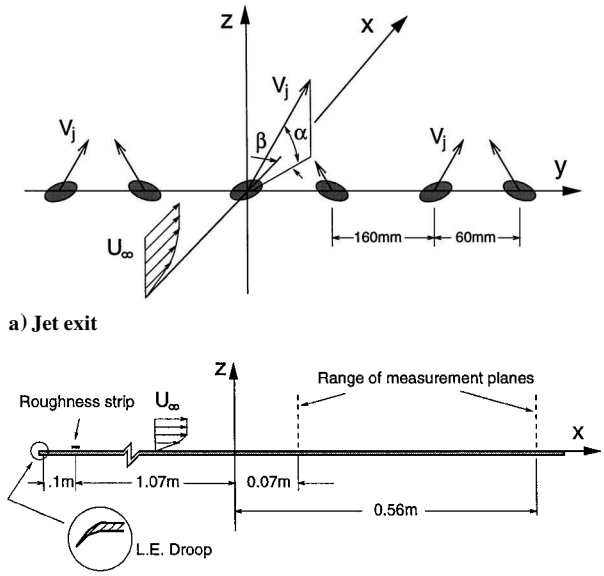

a) Jet exit

b) Plate dimensions

Fig. 1 Schematic.

B. LDA Measurements

The LDA measurements were performed with a three-component Dantec system with a 5-W Ar-ion laser generator. The LDA system was operated in an off-axis backscatter mode. A description of the velocity resolution can be found in Ref. 7. The velocities measured in the beam axes were resolved into the tunnel coordinate system (x, y, z) using a matrix transformation. Seeding was provided by two seeding generators: one released seed particles downstream of the model and the other into the nozzle flow. The seeding in the nozzle flow was released into the flow after the Fisher valve. The long distance between the seeding release and nozzle exit minimized possible bias. The number of measurement points in a crossflow plane ranged from 490 to 520. The measurement grid spacing varied, ranging from 2 mm near the center of the vortex to 8 mm away from the vortex pairs. The nearest sampling point to the wall was 0.95 mm. The LDA signals were analyzed using three Dantec Burst Spectrum Analyzers. On average, a total of 2000 bursts (instantaneous samples) were collected for each point. Results are presented in terms of velocity contours, cross-plane vectors, and streamwise vorticity. Natural cubic splines were used to obtain the derivatives of U, V, W with respect to the measurement coordinates x, y, z. The circulation level is given as

$$\Gamma = \int_y \int_z \Omega \, \mathrm{d}\frac{y}{D} \, \mathrm{d}\frac{z}{D}$$

In calculating the circulation level the nondimensional vorticity data with $|\Omega| < 0.05$ were ignored. This practice ensured that the noise in the measured data would not mask the overall circulation.

C. Errors and Uncertainties

The errors and uncertainties were estimated for the measured properties. The positional accuracy of the LDA traverse mechanism was ±0.01 mm. However, the uncertainties in determining x, y, z were estimated at ±0.15 mm taking into account the gear backlash. The LDA beam measurement volume had a cross-section diameter of 0.326 mm. The conclusion was made that the uncertainties in the x, y, z measurements were ±0.16 mm. Uncertainties in the pitch and skew angles of the jet were ±0.25 deg. The flow temperature variation during a test run was ±1.5°C. The tunnel speed was maintained to an accuracy of ±0.05 m/s. Following the procedure given by Moffat,[11] the uncertainties in the velocity measurements were estimated at ±0.09, ±0.31, and ±0.09 m/s for the three velocity components U, V, and W, respectively, at the freestream speed of 20 m/s.

For the turbulent stress measurements an estimation of the 95% confidence interval was obtained following the procedures given by Benedict and Gould.[12] Typical values are $\overline{uu}$, $\overline{ww} < \pm 13\%$; $\overline{vv}$, $\overline{uv}$, $\overline{vw} < \pm 16\%$; and $\overline{uw} < \pm 13\%$. As the number of samples varied in the measurement, the estimation of the final uncertainties was difficult. The preceding numbers represented the worst cases. In general, around the center of the vortex and near the wall the uncertainties were higher because of a lack of seeding. The smoothness of the results suggested that the actual uncertainties were lower than the numbers just quoted.

III. Results and Discussion

A. Flow Around the Nozzle Exit

In studying the development of the streamwise vortices and their effectiveness, attention has been paid to the area around the nozzle exit, where the spanwise moment of a skewed jet is converted to streamwise vorticity. It is in the area immediately after the nozzle exit that the turbulent stress production is strongest.[13] Principal flow

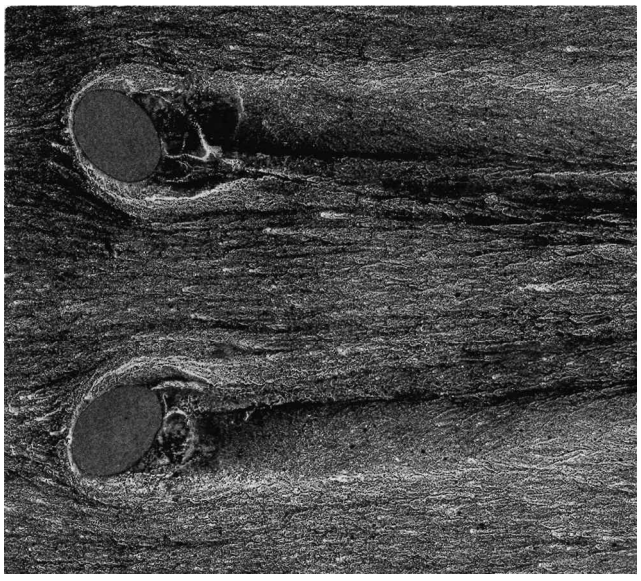

$\lambda = 0.5$

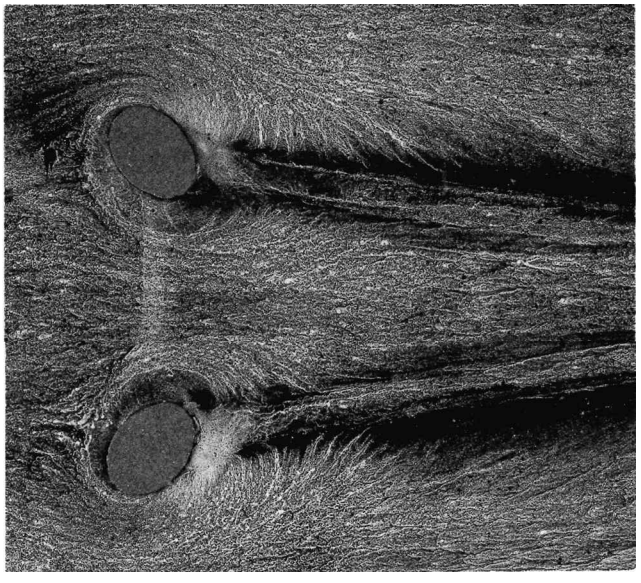

$\lambda = 1.5$

Fig. 2 Oil flows.

phenomena such as separation, entrainment, and turbulent mixing in the wake of the jet all contribute toward the formation of the final trailing vortex behind each nozzle. Some features of the flow can be observed through surface flow visualization. In Fig. 2 oil flows at $\lambda = 0.5$ and 1.5 are presented. (The $\lambda = 1.0$ case is similar to the $\lambda = 1.5$ case.) The major features do not differ significantly from those of a single jet.[7] The present arrangement of the nozzle, though, does bring about specific features, as each streamwise vortex is influenced by the adjacent counter-rotating vortex. In front of the nozzle, the oil flow seems to reveal an area of flow separation, pointing to the possible existence of a horseshoe vortex and roll-up of the vortex around the exit. Caution, however, should be exercised in interpreting this feature, as efforts to identify the detailed structures of the flow in this region are yet to confirm flow separation. Two possibilities exist: 1) the separation is confined to a thin region above the aerodynamic surface, and 2) there is an accumulation of oil because of flow deceleration approaching the jet exit. This anomaly merits further attention in model tests and numerical modeling attempts. The oil flow behind the nozzle also reveals a slight difference between the flows at $\lambda = 0.5$ and those at 1.0 and 1.5. At $\lambda = 0.5$ the jet flow after the nozzle exit seems to turn away from the skew direction into the flow direction, which is then followed by flow entrainment. This effect, though still present, is rather small at $\lambda = 1.0$ and 1.5. Instead we see a strong flow entrainment. The spanwise flow generated by the streamwise vortices follows downstream. The oil flow also indicates flow recirculation just behind the nozzle exit (with accumulation of oil).

As the oncoming turbulent boundary-layer flow is turned around the nozzle, it experiences separation (Fig. 2). This effect is much more pronounced on the downwash side (see also later LDA results). Farther downstream, the vortices created by the nozzle pair are seen to move toward each other. At $\lambda = 0.5$ the precise feature is not clear. This process ends around $x = 20D$ when the relative spanwise positions of the vortex experience only small movement.

Velocity measurement was conducted at a plane parallel to the aerodynamic surface at $z = 0.25D$. This area relates to the so-called near field, where the vortex is being generated and the wake of the jet is still a prominent feature of the flow. In the present study we have noticed large variations in the jet flow velocity immediately outside the nozzle exit, which obviously will exert a substantial influence on the characters of the vortex. The momentum flux rate of the jet is determined by the nozzle flow and its interaction with the oncoming boundary layer. We have therefore selected the jet velocity (mass flow rate of the jet) as a varying parameter in the tests. In a tunnel test this parameter can be easily controlled/regulated (see Sec. II.A). Provided that the nozzle geometry is known, the jet velocity ratio λ seems to be a better choice and can be used in a numerical model. In Figs. 3–5 the velocity vectors, the total velocity, and turbulent kinetic energy (TKE) contours are presented.

In front of the nozzle, the direction of the velocity vectors give no evidence of flow separation at this height. The aforementioned turning of the jet flow is clearly observed at this height as well. This feature is strong at $\lambda = 0.5$ but also exists at $\lambda = 1.0$ and 1.5. The spanwise velocity observed after the nozzle exit on the downwash side points to strong flow entrainment induced by the jet and, farther downstream, the induced velocity of the vortex. The existence of flow separation immediately after the nozzle exit is not shown in the velocity vectors at this height. However, measurements closer to the surface do reveal regions of flow recirculation downstream of the nozzle exit. A velocity survey at a height of $z = 0.125D$ confirms some observations made earlier (not shown). First, the flow approaching the nozzle decelerates. Flow separation, if it exists, is confined to a thin region above the surface. Second, the flow after the nozzle is characterized by recirculation and strong entrainment.

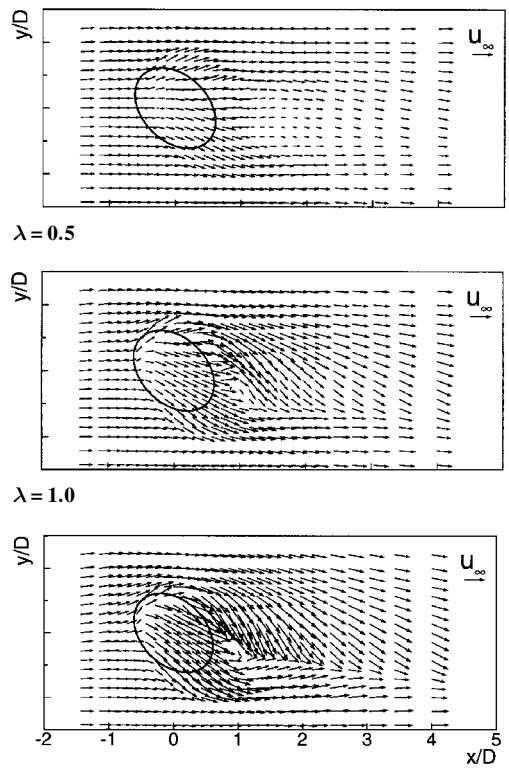

Fig. 3 Velocity vectors of the flow around the jet exit: $z/D = 0.25$.

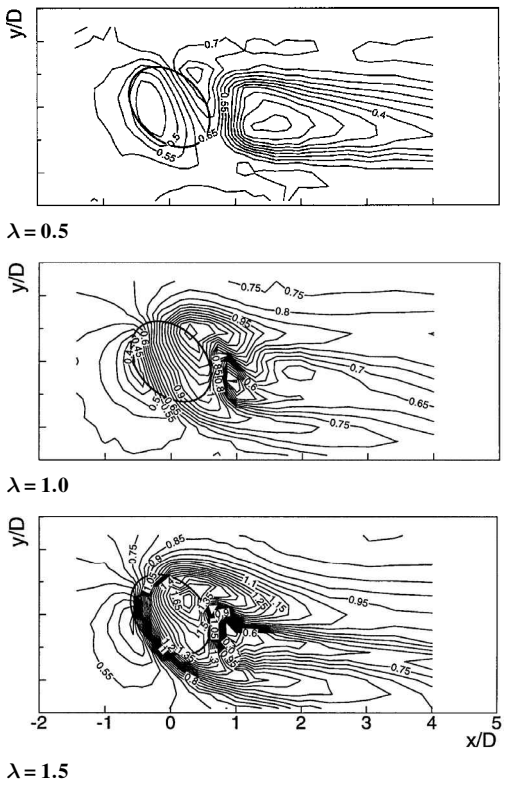

Fig. 4 Total velocity $\sqrt{(U^2 + V^2 + W^2)}/U_\infty$: contours of the flow around the jet exit; $z/D = 0.25$.

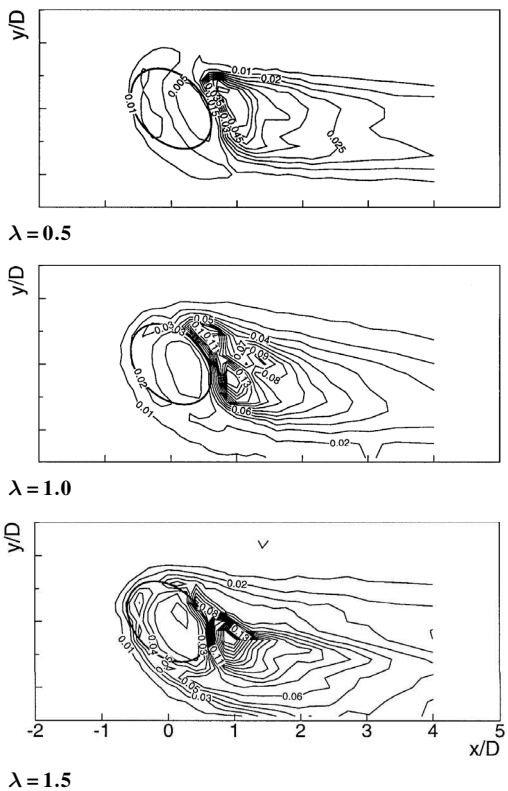

Fig. 5 TKE: contours of the flow around the jet exit; $z/D = 0.25$.

In the total velocity contours (Fig. 4) the low-speed region in front of the jet corresponds to the flow deceleration and a high pressure. The high-velocity region corresponds to the core of the skewed jet. The highest total velocity in the core of the jet is always higher that the mean jet velocity. The highest velocity contour corresponds to $\sqrt{(U^2 + V^2 + W^2)}/U_\infty = 0.8$ at $\lambda = 0.5$, 1.3 at $\lambda = 1.0$ and 1.7 at $\lambda = 1.5$. This feature is associated with the fully developed nozzle flow and an acceleration of the jet flow in the core region. In the area following the core of the jet, the flow velocity is rather small, and large-scale turbulence mixing, which is associated with the flow separation, occurs.

B. Counter-Rotating Vortices

A clear understanding of the vortex development should contribute to a better implementation of the device in terms of location. Single-jet studies[4,7] have shown that a primary streamwise vortex will eventually be formed after each skewed nozzle, regardless of the initial vorticity field in the vicinity of the nozzle exit. The vortex development could be divided into two stages: 1) a near field, where the wake of the jet is still prominent, and 2) a far field, where the dominant physics is turbulent dissipation and diffusion. The present flow retains principal features of the single-jet flow.

Two features characterize this particular fluid flow: 1) the diametrically opposed, spanwise moments of the jets and 2) the upwash between the vortices. The directions of the initial spanwise moments of the jets ensure that the streamwise vortices move toward each other in the initial stage of the vortex development, where the effect of the jet/wake is still prominent. In between the vortex pair, the counter-rotating vortices create the upwash region, which is limited by the positions of the vortices. Outside the upwash region the vortices generate downwash of the secondary vortex flow. The downwash effect is favorable for flow control. The arrangement of the jets therefore leads to a secondary vortex flowfield in the boundary layer whereby the upwash is limited and downwash maintained. The favorable effect, of course, depends on a proper separation between the vortex pairs in a practical application where an array of jets is used.

The streamwise movement of the vortices is shown in Figs. 6–8 with secondary velocity vectors at $\lambda = 0.5, 1.0$, and 1.5. In Figs. 9–11 the corresponding streamwise velocity contours (viewed from upstream) are given. In the measurements the clockwise-rotating vortex (left-hand vortex viewed from upstream) of the vortex pair is measured with finer sampling grid points than the right-hand one. Therefore our discussion will concentrate on this vortex. The secondary velocity vectors show clearly the counter-rotating vortex pair, which is embedded inside the boundary layer. In the case of $\lambda = 1.5$ flow, the vortices are located near the edge of the boundary layer as they move downstream. Under all of the test conditions, the center of the vortex moves gradually away from the wall, and no sudden jump in position or meandering is observed (see also later discussions). In the secondary velocity vectors one can also observe the counter movement of the vortices caused by the initial spanwise moments of the jets. At $\lambda = 1.0$ and 1.5 this movement is large until $x = 20D$ when the relative positions of the vortices experience only small variations. In between the vortices a symmetric plane is established, and there exists a general upwash of the

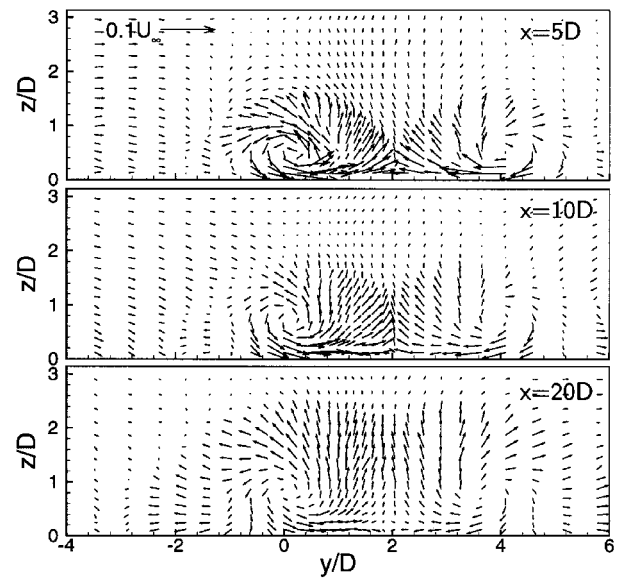

Fig. 6 Cross-plane velocity vectors at $\lambda = 0.5$.

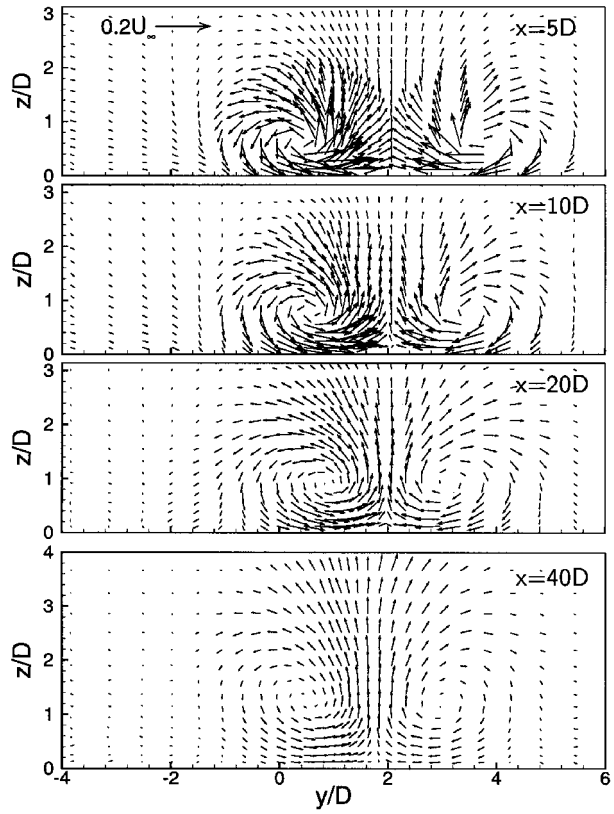

Fig. 7 Cross-plane velocity vectors at $\lambda = 1.0$.

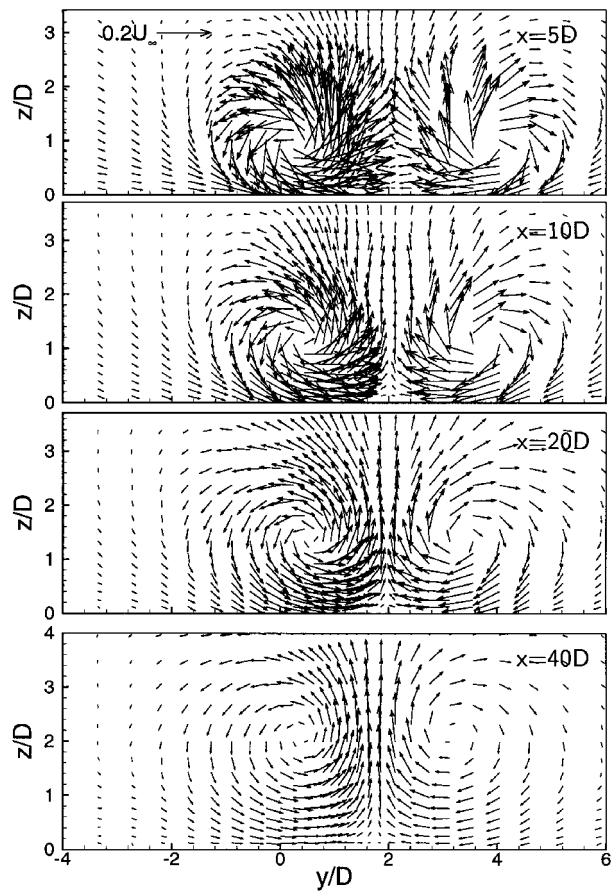

Fig. 8 Cross-plane velocity vectors at $\lambda = 1.5$.

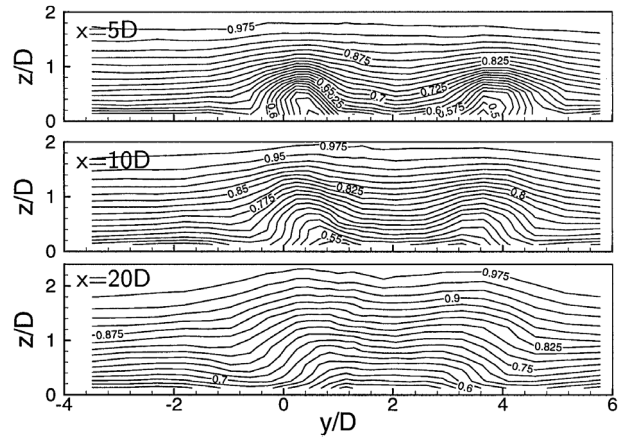

Fig. 9 Streamwise velocity U/U_∞ : contours at $\lambda = 0.5$.

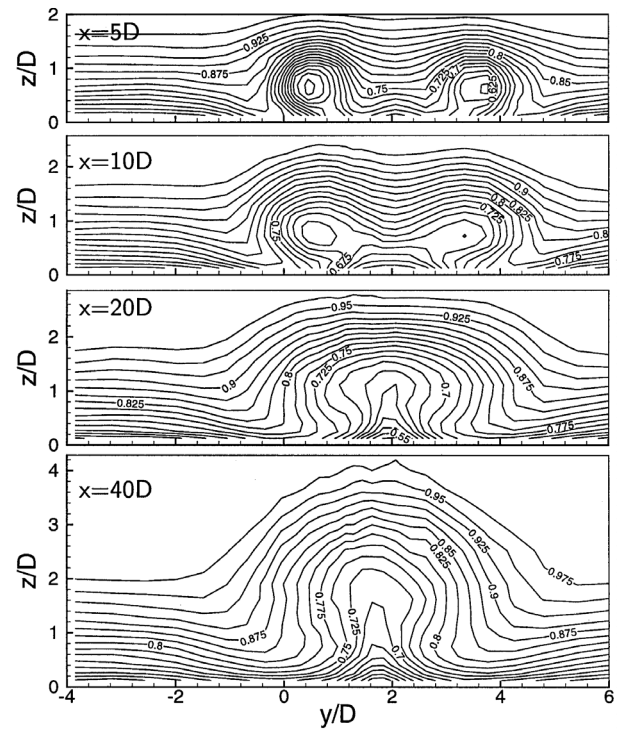

Fig. 10 Streamwise velocity U/U_∞ : contours at $\lambda = 1.0$.

secondary flow. The upwash of the secondary flow is stronger than that of a single-jet flow.[7] We can see that the upwash is limited by the centers of the vortices. Part of the upwash is indeed induced by the streamwise vortices. This particular flow, though, also has diametrically opposing, relatively strong near-wall spanwise flows, which lay directly underneath and to the upwash side of the vortex. The near-wall flows are caused by the jet and the presence of the wall, i.e., imagery vortex.[8] At least in the initial stage ($x < 20D$) of the vortex development, the effect is strong. As a result, a wall-jet type of flow exists. The interaction of the two near-wall flows creates a fountain-upwash effect, rather similar to that caused by multiple-jet ground impingement. This feature is clearly seen in Figs. 10 and 11, where the streamwise velocity contours at $x = 20$ and $40D$ show transverse movement of the flow in between the vortices as they moves toward each other.

The streamwise velocity contours show the influence of the wake of the jet at $x = 5$ and $10D$ at $\lambda = 1.0$ and $x = 5$, 10, and $20D$ at $\lambda = 1.5$. This feature is indicated by the areas occupied by the concentric contours in Figs. 10 and 11. This influence of the jet can be observed much clearer in the TKE contours in Figs. 12–14. In the TKE contours this influence is indicated by the concentric contours as well, which can be observed at up to $x = 20D$. A high turbulent mixing level is observed in the areas occupied by the concentric

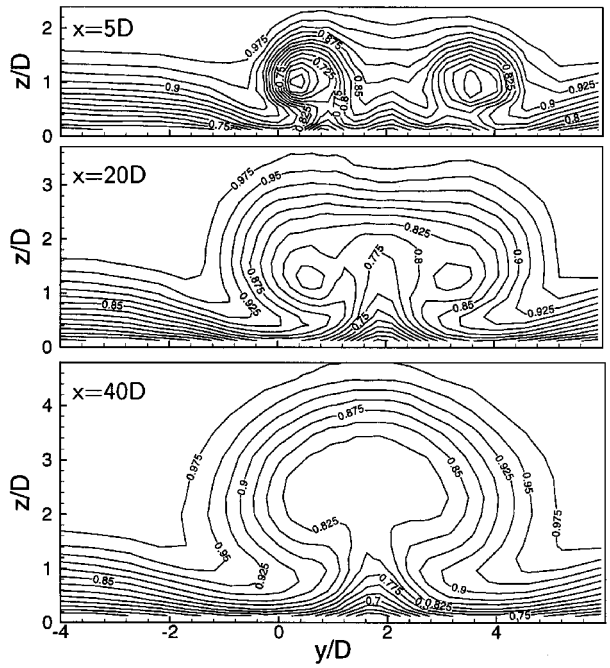

Fig. 11 Streamwise velocity U/U_∞ : contours at $\lambda = 1.5$.

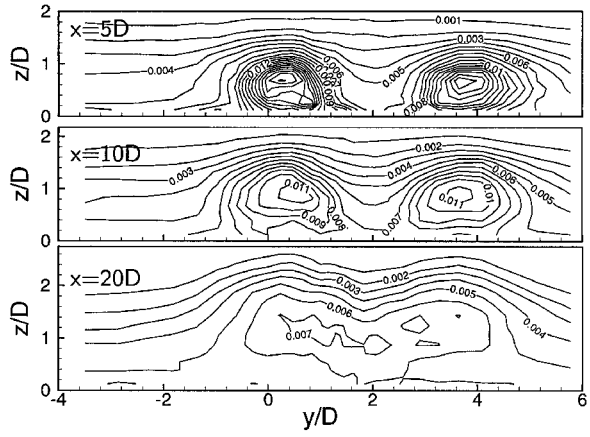

Fig. 12 TKE contours at $\lambda = 0.5$.

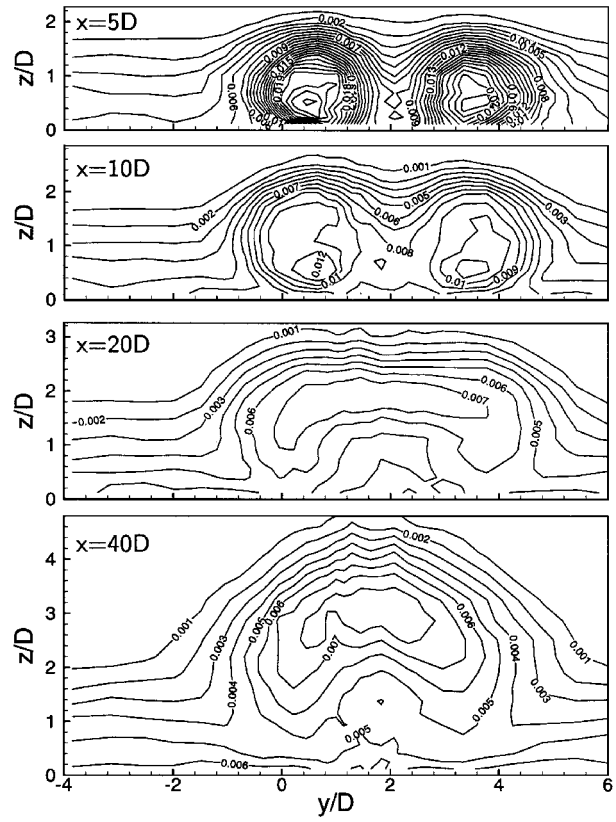

Fig. 13 TKE contours at $\lambda = 1.0$.

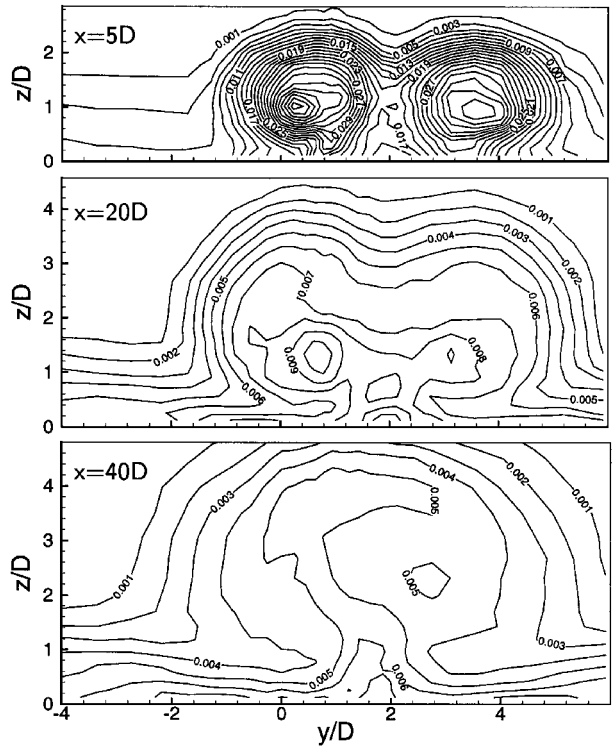

Fig. 14 TKE contours at $\lambda = 1.5$.

contours, i.e., the wake of the jet. After $x = 20D$ the separate areas of the concentric contours merge. At $x = 5D$ the level of TKE is substantially higher than that at $x = 20D$, which can be viewed as the demarcation line between the near field and the far field of the vortex development. The peak TKE level drops by as much as two times from $x = 5$ to $20D$ at $\lambda = 0.5$, three times at $\lambda = 1.0$, and 4.5 times at $\lambda = 1.5$.

In this study we have employed terms such as *near field* and *far field* to describe the vortex evolution. In the near field the jet is still exerting a significant influence, and in the far field the dominant physics in the vortex development is the turbulent dissipation and diffusion. An effective method in characterizing the vortex development is to use the spanwise velocity distribution, as opposed to the primary (streamwise) velocity or surface pressure. In Fig. 15 the spanwise distributions of the spanwise velocity are given for the three test cases at a height of $z = 0.25D$. The spanwise variation of the spanwise velocity is associated with the strength of the streamwise vortex. At $\lambda = 0.5$ the effect of the vortex flow can still be seen at $x = 30$ and $40D$. The basic characteristics, though, remain the same as those at $x = 20D$. Several features are worth noting here. First, the spanwise velocity shows two peaks with opposite signs, corresponding to the two counter-rotating vortices. At $x = 5$ and $10D$ there is evidence of two small peaks of opposite signs in between the two large ones (Fig. 15a). These two small peaks are associated with the induced vorticities caused by the rolling up of the initial jet, which are quickly engulfed by the primary vortex after each inclined jet. Second, the spanwise velocity distributions after $x = 20D$ are consistent with two primary vortices. Up to $x = 20D$, there is a quick reduction of the peak spanwise velocity as the vortices move downstream. After $x = 20D$ the streamwise variation of the spanwise velocity is rather small, suggesting that the vortices have been established and the main flow physics are now the turbulent dissipation and diffusion. Third, a spanwise movement of the main vortex is indicated by

Table 1 Vortex development

	$\lambda = 0.5$			$\lambda = 1.0$					$\lambda = 1.5$				
x/D	5	10	20	5	10	20	30	40	5	10	20	30	40
Ω_c	−0.280	−0.113	−0.082	−0.879	−0.463	−0.205	−0.116	−0.109	−1.678	−0.994	−0.461	−0.316	−0.206
y_c/D	0.150	0.131	0.082	0.350	0.577	0.872	0.745	0.505	0.260	0.396	0.549	0.528	0.380
z_c/D	0.475	0.709	0.811	0.617	0.788	0.904	1.152	1.273	0.950	1.149	1.396	1.772	2.105
Ω_m	−0.465	−0.213	−0.104	−1.108	−0.594	−0.296	−0.175	−0.136	−1.936	−1.083	−0.479	−0.386	−0.251
y_m/D	0.235	0.249	0.460	0.450	0.839	1.143	1.143	1.143	0.442	0.442	0.624	0.786	0.624
z_m/D	0.250	0.376	0.398	0.539	0.555	0.733	0.748	1.150	0.850	1.082	1.115	1.628	2.316
Γ	−0.177	−0.109	−0.065	−0.647	−0.551	−0.390	−0.313	−0.237	−1.353	−0.986	−0.790	−0.700	−0.583

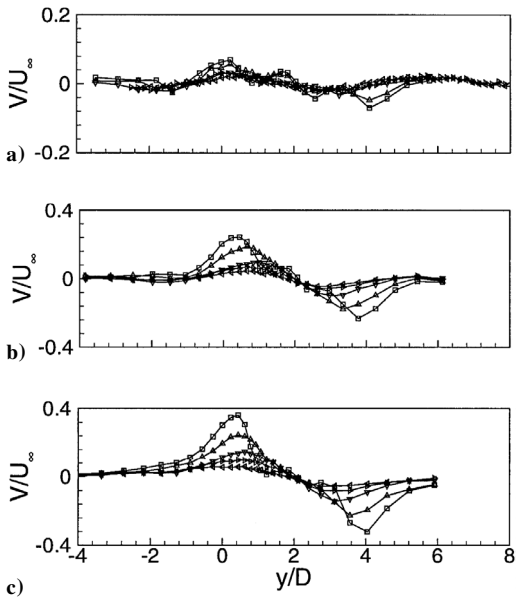

Fig. 15 Spanwise velocity variations at $z = 0.25D$: a) $\lambda = 0.5$, b) $\lambda = 1.0$, and c) $\lambda = 1.5$. Symbols: ▮, $x/D = 5$; △, $x/D = 10$; ▽, $x/D = 20$; ▷, $x/D = 30$; and ◁, $x/D = 40$.

the movement of the peak spanwise velocity. Before $x = 20D$ the vortices are seen to move toward each other. After $x = 20D$ the variation in the spanwise location of the peak velocity is small and in the opposite direction to that before $x = 20D$. This feature confirms the earlier observation of $x = 20D$ as the demarcation line of the vortex development, which is the same as that of a single-vortex flow.

The measured properties of the vortex are listed in Table 1, including the position, the peak vorticity, and the circulation level. The center of the vortex is defined in this study as the geometry center of the concentric secondary flow streamlines. The location of the peak vorticity coincides with the geometry center of the concentric vorticity contours of the main vortex. Both locations can be defined for the flows in this study and are therefore used in the discussion of the results. The peak vorticity appears beneath the center of the vortex because of the presence of the wall (mirror vortex)[8] and is always located to the upwash side. The location of the vortex suggests that the primary vortex is indeed embedded inside the boundary layer. In the transverse direction the center of the vortex z_c moves away from the wall monotonically. In the case of the $\lambda = 1.5$ flow, it moves to the edge of the otherwise flat-plate boundary layer at $x = 40D$. Compared to a single-jet flow at the same test conditions, the center of the vortex moves farther away from the wall. For example, at $\lambda = 1.0$, the center of the vortex is located at $z_c/D = 1.273$ at $x = 40D$, compared to 1.079 for the single-jet flow. At $\lambda = 1.5$ the center of the vortex is located at $z_c/D = 2.105$ at $x = 40D$, compared to 1.697 for the single-jet flow. The presence of the counter-rotating counterpart in the vortex pair obviously contributes to the difference. In the spanwise direction the vortex does not move monotonically in one direction because of the limiting presence of the other vortex. As observed in the oil flow, the vortex moves initially in the skewed direction of the jet nozzle. The rate of spanwise movement is slower than a single-jet flow. Before $x = 20D$ the initial moment of the jet leads to the spanwise movement of the vortex. As discussed earlier, a mature vortex is established at around $x = 20D$, where the influence of the jet is reduced. The vortices then begin to move apart in the spanwise direction. This is reflected in the y_c value listed in Table 1.

The peak vorticity at the center of the vortex decreases downstream. The value of the peak vorticity Ω_c changes differently with the three jet velocity ratios. At $\lambda = 0.5$ and 1.0, Ω_c is higher than the single-jet value. For example at $x = 20D$, Ω_c is −0.082 compared with −0.072 for the single-jet flow at $\lambda = 0.5$. At $\lambda = 1.0$, Ω_c is −0.205 compared with −0.156 for the single-jet flow. The behavior is different at $\lambda = 1.5$. The peak value is generally lower than that of the single-jet flow. For example at $x = 20D$, Ω_c is −0.461 compared with −0.612 for the single-jet flow. This feature shows the importance of the relative positions of the vortices, hence nozzle locations and orientation, and the need to optimize the geometry setup for a practical application. The difference between the flows at $\lambda = 0.5$ and 1.0 to that at $\lambda = 1.5$ lies in the level of the interaction between the diametrically opposed near-wall flow generated by the counter-rotating vortices. An ideal arrangement should ensure a full development of the individual vortex and enhancement of the vortex by its counter-rotating counterpart. At $\lambda = 1.5$ and with the current nozzle separation, the two primary vortices move quickly toward each other. The merging of the two vortices occurs before the full establishment of the vortex. In Figs. 11 and 14, one can see that while the wake of the jet is still prominent (at $x = 20D$), the two vortices are beginning to merge. As a result, a strong fountain-upwash effect is present. The interaction of the diametrically opposed near-wall flows creates a local high turbulent mixing region in between the two vortices near the wall (Fig. 14), which is not present at $\lambda = 0.5$ (see Fig. 12). The local high turbulent mixing does not contribute to the enhancement of the vortex.

IV. Conclusion

An experimental study was performed on counter-rotating streamwise vortices generated by inclined jets in an otherwise flat-plate turbulent boundary layer. Measurements were performed with a three-component LDA system in a low-speed wind tunnel. The effects of jet velocity and streamwise development of vortex were investigated. The study helped to improve the current understanding of inclined jet in a crossflow. Specifically, we found the following:

1) Two counter-rotating primary vortices are produced by the inclined jets that are embedded in the turbulent boundary layer.

2) The secondary flow in between the vortices is characterized by an upwash region. The upwash is caused by the vortices and the interaction between the diametrically opposed near-wall flows, which leads to a fountain-upwash effect.

3) Flow separation and entrainment are observed behind the jet exit.

4) The development of the streamwise vortex can be divided into near field and far field, where the demarcation line is approximately $x = 20D$. In the near field the wake of the jet is still prominent. In the far field turbulent dissipation and diffusion play important roles.

5) The vortices move monotonically away from the wall as they develop downstream. In the spanwise direction the vortices first move toward each other before $x = 20D$ and then move away from each other.

6) Compared with the corresponding single-jet flow, the $\lambda = 0.5$ and 1.0 flows have higher peak vorticity, and the $\lambda = 1.5$ has a lower peak vorticity at the center of the vortex.

Acknowledgments

The study is supported under EPSRC Grant GR/J17722. The author thanks M. Goodyer, A. Rona, and M. W. Collins for helpful discussions and assistance during the study.

References

[1]Wallis, R. A., "A Preliminary Note on a Modified Type of Air-Jet for Boundary-Layer Control," Aeronautical Research Council, CP-513, London, May 1956.

[2]Freestone, M. K., "Preliminary Tests at Low Speeds on the Vorticity Produced by Air-Jet Vortex Generators," Dept. of Aeronautics, City Univ., Research Memo. Aero. 85/01, London, Feb. 1985.

[3]Johnston, J. P., and Nishi, M., "Vortex Generator Jets—A Means for Flow Separation Control," *AIAA Journal*, Vol. 28, No. 6, 1990, pp. 989–994.

[4]Compton, D. A., and Johnston, J. P., "Streamwise Vortex Production by Pitched and Skewed Jets in a Turbulent Boundary Layer," *AIAA Journal*, Vol. 30, No. 3, 1992, pp. 640–647.

[5]Selby, G. V., Lin, J. C., and Howard, F. G., "Control of Low-Speed Turbulent Separated Flow Using Jet Vortex Generators," *Experiments in Fluids*, Vol. 12, No. 6, 1992, pp. 394–400.

[6]Zhang, X., and Collins, M. W., "Measurements of a Longitudinal Vortex Generated by a Rectangular Jet in a Turbulent Boundary Layer," *Physics of Fluids*, Vol. 9, No. 6, 1997, pp. 1665–1673.

[7]Zhang, X., and Collins, M. W., "Nearfield Evolution of a Longitudinal Vortex Generated by an Inclined Jet in a Turbulent Boundary Layer," *Journal of Fluids Engineering*, Vol. 119, No. 4, 1997, pp. 934–939.

[8]Westphal, R. V., Eaton, J. K., and Pauly, W. R., "Interaction Between a Vortex and a Turbulent Boundary Layer in a Streamwise Pressure Gradient," *Turbulent Shear Flow 5*, Springer–Verlag, Berlin, 1987, pp. 267–277.

[9]Cutler, A. D., and Bradshaw, P., "Strong Vortex/Boundary Layer Interactions, Part II. Vortices Low," *Experiments in Fluids*, Vol. 14, No. 6, 1993, pp. 393–401.

[10]Pauly, W. R., and Eaton, J. K., "Experiment Study of the Development of Longitudinal Vortex Pairs Embedded in a Turbulent Boundary Layer," *AIAA Journal*, Vol. 26, No. 7, 1988, pp. 816–823.

[11]Moffat, R. J., "Describing the Uncertainties in Experimental Results," *Experimental Thermal and Fluid Science*, Vol. 1, No. 1, 1988, pp. 3–17.

[12]Benedict, L. H., and Gould, R. D., "Towards Better Uncertainty Estimates for Turbulence Statistics," *Experiments in Fluids*, Vol. 22, No. 2, 1996, pp. 129–136.

[13]Zhang, X., "Turbulence Measurements of a Longitudinal Vortex Generated by an Inclined Jet in a Turbulent Boundary Layer," *Journal of Fluids Engineering*, Vol. 120, No. 4, 1998, pp. 765–771.

J. C. Hermanson
Associate Editor